UNIVERSITÀ DEGLI STUDI DI TORINO

Granato L, Longo D, Boutry S, Vander Elst L, Henoumont C, Aime S, Muller RN, Laurent S

Synthesis and Relaxometric Characterization of New Poly[N,N-bis(3-aminopropyl)glycine] (PAPGly) Dendrons Gd-Based Contrast Agents and Their in Vivo Study by Using the Dynamic Contrast-Enhanced MRI Technique at Low Field (1T)

In Chemistry & Biodiversity

The definitive version is available at:

DOI: 10.1002/cbdv.201900322

Synthesis and relaxometric characterization of new Poly[N,N-bis(3-AminoPropyl)Glycine] (PAPGly) dendrons Gd-based contrast agents and their in-vivo study by using the Dynamic Contrast-Enhanced MRI technique at Low field (1 T)

L. Granato,[1] D. Longo,[4] L. Vander Elst,[1] C. Henoumont,[1] S. Aime,[2] R.N. Muller,[1,3] S. Laurent[1,3]

[1] General, Organic and Biomedical Chemistry Unit, NMR and Molecular Imaging Laboratory, University of Mons, 19 avenue Maistriau B-7000 Mons, Belgium

[2] Department of Molecular Biotechnology and Health Sciences, University of Torino, Torino Italy

[3] Center for Microscopy and Molecular Imaging, 8 rue Adrienne Bolland, B-6041 Charleroi, Belgium

[4] Institute of Biostructures and Bioimaging (IBB); Italian National Research Council (CNR); Torino, Italy

Abstract

The synthesis of poly[N,N-bis(3-aminopropyl)glycine] (PAPGly) dendrons Gd-based contrast agents (GdCAs) via an orthogonal protection of the different functional groups and an activation/coupling strategy wherein a specific number of synthetic steps adds a generation to the existing dendron have been described. The aim of this protocol is to build up two different generations of dendrons (G-0 or dendron's core, and G-1) with peripheral NH_2-groups to conjugate a 1,4,7,10-tetraazacyclododecane-1,4,7-triacetic acid (DO3A) derivative and after to chelate with Gd^{3+} paramagnetic ions. These complexes, which have a well-defined molecular weight, are of relevance to MRI as an attempt to gain higher ^1H relaxivity by slowing down the rotation of molecule compared to monomeric Gd(III) complexes used as contrast agents and to increase the number of paramagnetic centers present in one molecular structure. From the study of their water ^1H longitudinal relaxation rate at different magnetic fields (NMRD, Nuclear Magnetic Relaxation Dispersion) and by evaluating the variable temperature ^{17}O NMR data we determined the parameters characterizing the water exchange rate and the rotational correlation time of each complex, both affecting ^1H relaxivity.

Furthermore, these two novel PAPGly GdCAs were objects of i) an in-vivo study to determine their biodistributions in healthy C57 mice at several time points, and ii) of the Dynamic Contrast-Enhanced MRI (DCE-MRI) approach to assess their contrast efficiency measured in the tumour region of C57BL/6 mice transplanted subcutaneously

with B16-F10 melanoma cells. The aim of the comparison of these two dendrons GdCAs, having different molecular weights (MW), is to understand how the relationship between MW and relaxivity may influence the contrast enhancement capabilities in vivo at low magnetic field (1 T). Significant contrast enhancement was observed in several organs (vessel, spleen and liver), already at 5 min post-injection, for the investigated CAs. Moreover, these CAs induced a marked contrast enhancement in the tumour region, thanks to the enhanced permeability retention effect of those macromolecular structures.

Introduction

Magnetic resonance imaging (MRI) has become a powerful non-invasive diagnostic imaging modality that provides high-quality anatomic images and other physiologic data. Its advantages include a high spatial resolution, a non-ionizing radiation source, and the ability to extract, simultaneously, physiological and anatomical information of soft tissue (1, 2). However, a major limitation of MRI remains its inherent low sensitivity. To increase the sensitivity of MRI, scientists have developed non-toxic contrast agents (CAs) over the last few decades, which are administered to the patient to enhance image contrast between normal and diseased tissue or to indicate the status of organ function or blood flow (3,4). The development of new MRI contrast agents offers intriguing challenges for investigators in the chemical, physical, and biological sciences, including the design and synthesis of stable, non-toxic, and tissue-specific metal complexes and the understanding of their effect on relaxation behaviour in solution and in tissues. These biocompatible contrast agents alter the longitudinal (T_1) and transverse (T_2) relaxation times of the surrounding water protons, therefore enhancing image contrast in tissues of interest. For this reason, MRI CAs are generally categorized as T_1 and T_2 CAs based on their magnetic properties and relaxation mechanisms. Gadolinium chelates are effective for increasing T_1 relaxation rate ($1/T_1$) and commonly used as T_1 CAs, generating a positive image contrast (5). Superparamagnetic iron oxide nanoparticles are more effective for increasing T_2 relaxation rate ($1/T_2$) and commonly used as T_2 CAs, producing negative image contrast (6).

Clinical MRI contrast agents are low molecular weight complexes that have transient tissue retention due to their short half-life. These agents are nonspecific, extravagate rapidly from blood circulation and distribute throughout the extracellular space of normal and diseased tissues. Their unfavourable pharmacokinetic profile makes these agents unsuitable for MR angiography and for the early detection of cancer tissue. In addition, these low molecular weight complexes show some restrictions to reach the ideal (or maximum attainable) relaxivity (7).

In fact, the rapid extravasation of low MW contrast agents causes a fast decrease in their concentration in the bloodstream after administration. As a consequence, this not only result in a lower signal enhancement in the normal blood vessel, but also in a higher background signal from the surrounding tissue. An increase in the background signal may reduce the spatial resolution such that blood vessels can no longer be discriminated from their surroundings. Contrary to low MW contrast agents, high MW contrast agents remain in high concentrations in the bloodstream. Due to the fact that high MW contrast agents show little extravasation and long intravascular retention, they are commonly referred to as blood pool agents, while low MW contrast agents are referred to as extravascular agents (7). First attempts to improve r_1, hence, contrast efficiency, was pursued by non-covalent binding of low MW contrast agents to the human serum albumin.

Secondly, low MW contrast agents rapidly diffuse from the bloodstream into the interstitial space, even in the case of healthy vessels. This relatively high permeability prevents their effective use in differentiating between benign lesions (normal vessels) and malignant tumours (hyperpermeable vessels) with contrast-enhanced MR imaging. On the other hand a better differentiation between these two types of vessels is possible with high MW contrast agents (8).

Thirdly, low MW contrast agents, such as Gd(III) complexes of 1,4,7,10-tetraazacyclododecane-1,4,7,10-tetraacetic acid (DOTA), contain typically one Gd^{3+} ion per molecule. Consequently, the relatively low signal enhancing effect (or longitudinal relaxivity r_1, s^{-1} mM^{-1}) requires that high concentrations (*i.e.* high doses) of MRI contrast agent must be administered to eventually obtain sufficient contrast between the blood vessel and its surrounding tissue. A straightforward approach to increase the loading of Gd^{3+} per molecule is to attach multiple Gd(III) chelates to a macromolecular scaffold. An additional advantage of (covalently) attaching multiple Gd(III)-based complexes to high MW structures is the strong increase in r_1 per Gd^{3+} as a result of the strong reduction in the molecular tumbling rate of the Gd(III) complex (7, 9).

Likewise of inulin-Gd-DO3A complexes (**10**), several natural and synthetic polymers, such as starch polysaccharide (11), dextran (12) or polylysine (13), have been modified and conjugated to contrast agents, and showed good efficiency in imaging. However, their use was limited because of synthetic and purification difficulties (polydispersity), low level of characterisation and non-reproducibility of the final chemical entities.

Dendrimers can offer several advantages as contrast agents compared to the traditional linear polymers. The dendritic architecture has a highly branched, three dimensional nanoscale structure with very low polydispersity, high functionality and inherent rigidity higher than the macromolecular linear polymers. Actually dendrimer-based contrast agents provide numerous benefits over low-molecular-weight

gadolinium chelates for MRI, including enhanced r_1 relaxivity (14,15) due to slow rotational dynamics, tunable pharmacokinetics that can be adapted for blood pool (16,17), liver, kidney, and lymphatic imaging, the ability to be a drug carrier, and flexibility for labeling due to their inherent multivalency (11, 18).

An important aspect for the *in vivo* application of these MRI contrast agents is that the relaxivity of Gd(III) complexes is field-dependent and, in the case of the paramagnetic macromolecular system, it shows a maximum efficiency at ca. 1 T (19, 20). The theory of paramagnetic relaxation describes well this experimental observation, since contrast agents with optimized water exchange rate (τ_M) show highest overall relaxivity at around 1 T, which is mainly controlled by the long rotational correlation time (τ_R) characteristic of the paramagnetic macromolecules (21). On the other hand, high fields provide an overall increase of the signal intensity (SI) that allows the rapid acquisition of highly resolved images.

The first dendrimeric MRI contrast agents were reported by Adam *et al.* (22) and Wiener *et al.* (23). Since then, many dendrimeric MRI CA have been reported using various dendrimers, including poly(amidoamine) (PAMAM) (25), poly(propylene imine) (PPI) (25, 26) and poly-L-lysine (PLL) (27). Dendrimeric Gd(III) complexes have showed higher relaxivity due to the more rigid structure than their linear polymeric counterparts (7, 28-30). Langereis *et al.* (25) reported that a Gd-DTPA conjugated to poly(propylene imine) dendrimer (the fifth generation G-5, Mw = 51 kDa) had r_1 relaxivity as high as 19.7 s^{-1} mM^{-1} per Gd(III) (1.5 T, 20 °C), which was 4.7 times that of Gd-DTPA. Dendrimer-based Gd(III) chelates were effective for contrast enhanced MRI of the kidneys, vasculature, liver, or tumour (31, 32). Here we report a "*convergent synthesis*" of poly[*N*,*N*-bis(3-aminopropyl)glycine] (PAPGly), as new dendrons Gd-based contrast agents. We describe the parameters governing the relaxivity of these new materials comparing them with those reported previously. We report also an *in-vivo* study in healthy mice and in mice with transplanted subcutaneously melanoma cells of those new PAPGly dendrons Gd-based contrast agents, having generation **G-0** and **G-1**, in order to determine and compare their biodistributions and contrast efficiency by Dynamic Contrast-Enhanced MRI (DCE-MRI) at low magnetic field (1 T).

Results and Discussion

Synthesis of poly[N,N-bis(3-aminopropyl)glycine] dendrons Gd-based contrast agents

The following approach described for the synthesis of these poly-amino-propyl-glycine (PAPGly) dendrons (Fig. 1) was based on the suitably convergent method of multibranched dendrimers synthesis mentioned above. We synthesised two different generations of dendrons **G-0** (or dendron's core) and **G-1**, via an orthogonal protection of the different functional groups and an activation/coupling strategy, wherein each synthetic step adds a generation to the existing dendron.

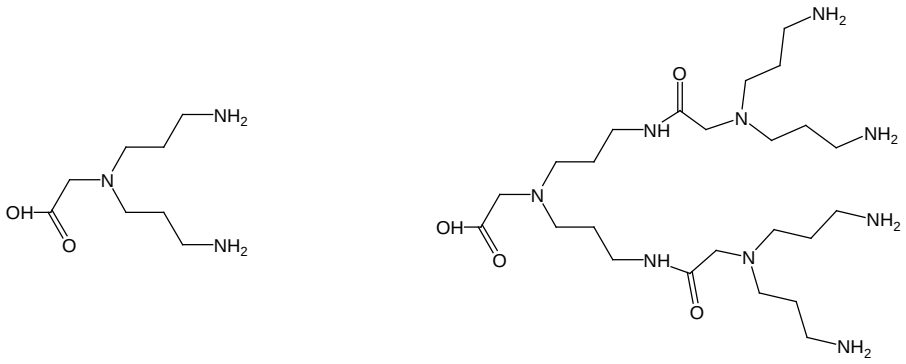

Dendron G-0 (or core) **Dendron G-1**

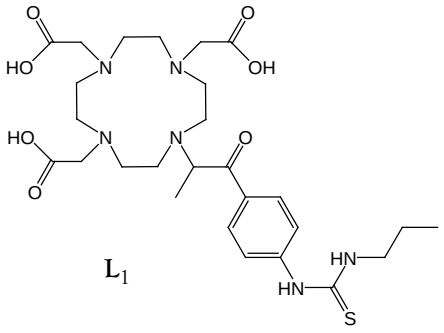

L_1

Figure 1: Chemical structures of ligand L_1 and the PAPGly drendrons with two different generations (**G-0**, **G-1**).

In the first step (Scheme 1), the primary amine functions in the commercially available polyamine 3, 3'-diaminodipropylamine **1** were protected using *t*-Boc groups producing compound **2** in 75% yield. The *t*-Boc group was used since it is stable toward hydrogenation and basic reaction conditions. In the next step, benzyl bromo acetate was used as alkylation reagent in the presence of DIEA using DMF as solvent. Purification of **3** by silica gel column chromatography using EtOAc/Heptane (70:30) as eluent produced white crystals in 90% yield. Removal of the benzyl protecting group of compound **3** was accomplished by hydrogenation at 60 psi using MeOH as solvent giving the deprotected polyamine derivative **4**. Subsequently the Boc group was removed by using TFA in DCM, to give the dendron **G-0**.

The ligand $\mathbf{L_1}$ (Fig. 1) was prepared via the synthetic route reported recently (33). The intermediate isocyanate-activated DO3A derivative (DO3A-NCSPP) of the chelate $\mathbf{L_1}$, freshly prepared, was used to conjugate with the dendron **G-0** in order to obtain the product **G-0**$(\mathbf{L_1})_2$.

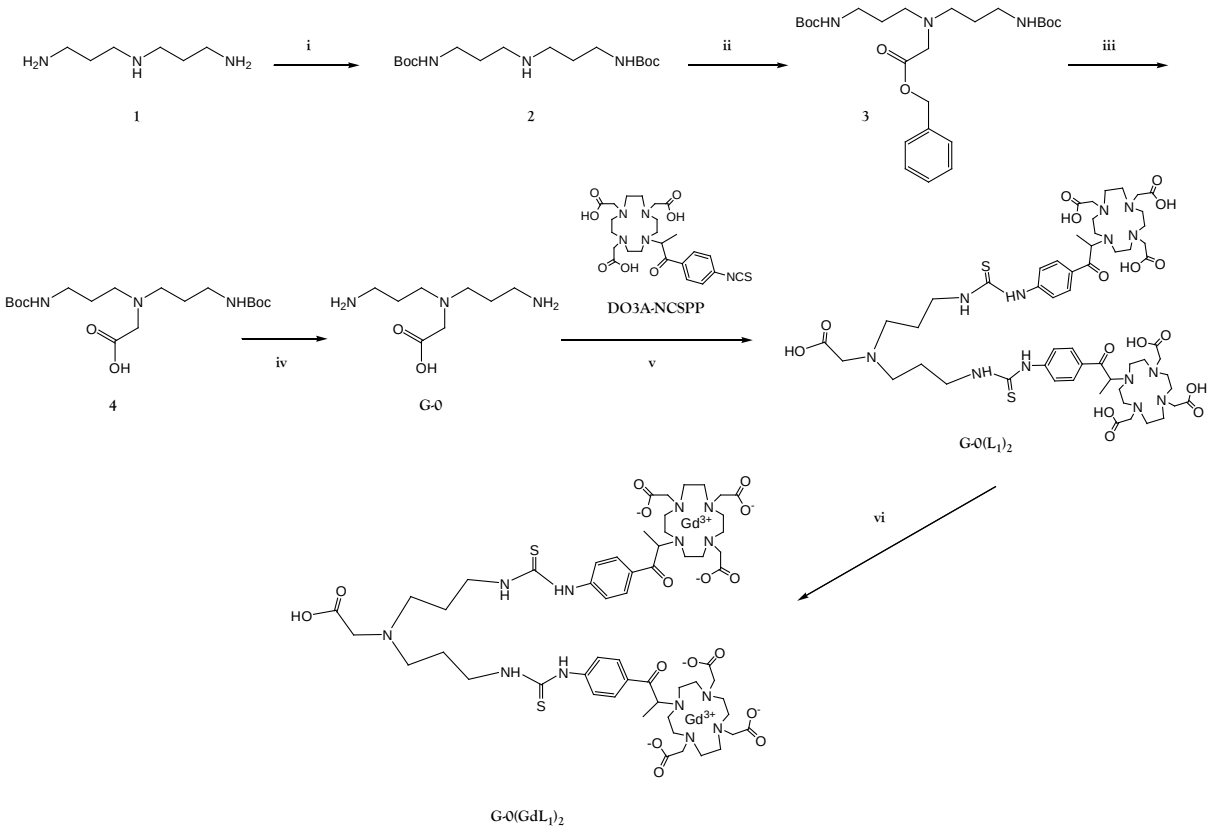

Scheme 1: Synthesis of dendron generation **G-0** (or core) and its gadolinium complex **G-0**$(\mathbf{GdL_1})_2$: (i) tert-butyl phenyl carbonate, DMF, room temperature (rt); (ii) benzylbromo acetate, DIPEA, DMF; (iii) Pd/C 10 %, MeOH, H_2 at 60 psi; (iv) CF_3COOH/CH_2Cl_2 50%, rt; (v) $CSCl_2$, CCl_4/water, rt; (vi) $GdCl_3 \cdot 6H_2O$, pH 6.5-7.0.

The generation one of the dendron (**G-1**) was efficiently synthesised in solution (CH_3CN) through the activation of the intermediate **5** (2.8 eq.) by using the reagent HATU, 1-[bis(dimethylamino)methylene]-1*H*-1,2,3-triazolo[4,5-*b*]pyridinium 3-oxid hexafluorophosphate, to generate an active ester from the carboxylic acid, and subsequent *N*-acylation with the primary amines of intermediate **4**, in the presence of DIPEA as organic base (Scheme 2). This typical peptide coupling leads the product **6**, which was purified by flash chromatography on silica gel using DCM/CH_3OH as mobile phase, obtaining a white crystal compound after evaporation of the solvent. The orthogonal deprotection of the carboxylic acid and the primary amine groups of compound **6** provide **G-1** dendron**,** by which its conjugation with the intermediate DO3A-NCSPP derivative of ligand $\mathbf{L_1}$ gives the product **G-1**$(\mathbf{L_1})_4$ (Scheme 2).

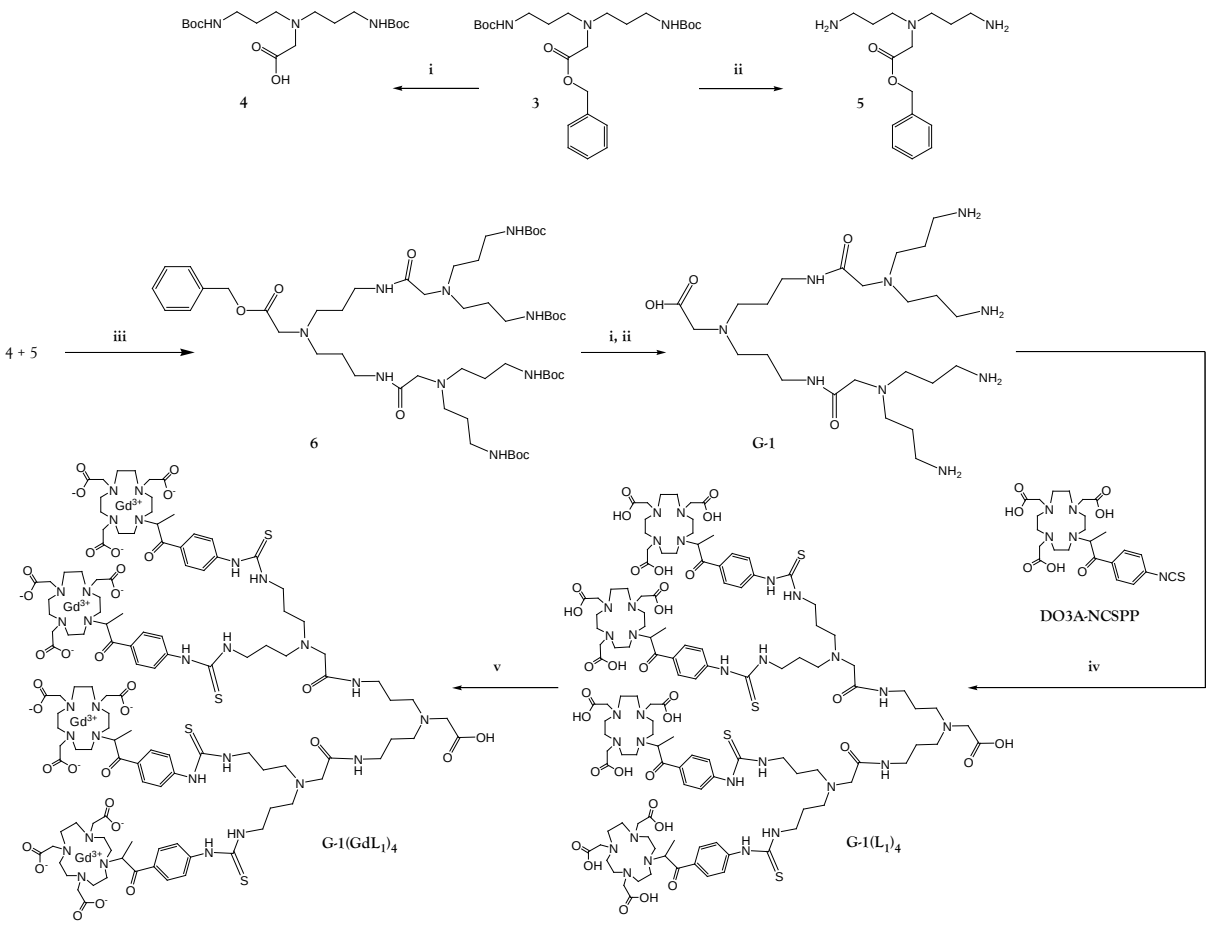

Scheme 2: Synthesis of dendron generation **G-1** and its gadolinium complex **G-1(GdL$_1$)$_4$**: (i) Pd/C 10 %, MeOH, H_2 at 60 psi; (ii) CF_3COOH/CH_2Cl_2 50%, rt; (iii) CH_3CN, HATU, DIPEA; (iv) $CSCl_2$, CCl_4/water, rt; (v) $GdCl_3 \cdot 6H_2O$, pH 6.5-7.0.

The Gd^{3+} complexes of both dendrons were prepared by adding stoichiometric amount of Gd^{3+} chloride to an aqueous solution of the ligands **G-0(L$_1$)$_2$** and **G-1(L$_1$)$_4$** (Schemes 1 and 2) while maintaining the pH of the solution between 6.5-7.0 by addition of 1 M NaOH aqueous solution. After 3-4 days the reaction mixture was stopped, and the excess of free lanthanide of dendron complex **G-0** was removed by centrifugation as $Gd(OH)_3$ precipitate, which appeared at pH 10 after addition of 1 M NaOH, whereas for **G-1** complex the free gadolinium was removed by membrane ultra-filtration. The absence of free Gd^{3+} ions was confirmed in both cases by a xylenol orange test.

Evaluation of the relaxivity and its parameters

The relaxivity depends on various factors including the external field, the number of coordinated water molecules, water exchange rate, rotational diffusion, first and second coordination sphere hydration, and the ion to water proton distance (9). DOTA-like chelates, such as the DO3A-*p*-aminophenyl-propan-1-one (10), have a single water molecule coordinated to the Gd^{3+} ion. Parameters such as the rate of the water exchange (τ_M) and the rotational dynamics of the molecule (τ_R) are most affected when attaching contrast agents to a polymer. Ideally for a small organic contrast agent, τ_M should be at maximum 10 ns and τ_R should be at least higher than 10 ns at a magnetic field of 1.5 T (most commonly used in clinical MRI scanners) (36). The results of relaxometric studies by fitting the ^{17}O NMR and ^{1}H NMRD data of the **G-0(GdL$_1$)$_2$** and **G-1(GdL$_1$)$_4$** dendrons complexes (Table 1) indicated an overall increase in relaxivity compared to the r_1 of the monomeric **GdL$_1$** complex previously studied (33) and of the commercial Gd-DOTA complex. As expected, the increase is the highest for the dendron agent at high generation (**G-1**) (Fig. 5b), with its relaxivity being 4 times higher than the monomeric macrocyclic Gd^{3+}poly(amino carboxylate) complex (Gd-DOTA and **GdL$_1$**, Table 1).

In order to determine the water exchange rate, a variable temperature ^{17}O NMR study was performed on the dendritic Gd^{3+}-complexes of the two different generations and on the monomeric complex. From the Table 1 and the Figure 5a, it appears there is no dramatic difference between the monomer and the **G-0(GdL$_1$)$_2$** complex, whereas for **G-1(GdL$_1$)$_4$** complex we can observe a somewhat longer water residence time. This is probably due to a steric constraint around the second coordination sphere of the Gd^{3+}-complex which limits the access to the water bulk to be coordinated to the paramagnetic centre. The study of ^{1}H NMRD profiles of these complexes, which take into account the second-sphere contribution, showed that the number of water molecules in the second-sphere (q_{ss}) is zero for the **G-1(GdL$_1$)$_4$** dendron complex comparing to the **G-0(GdL$_1$)$_2$**, where q_{ss} = 3 (Table 1). This is in line with the previous observation. As one of the most important outcomes of this study, we can thus confirm that the attachment of the macrocyclic unit to a large dendritic polymer molecule does not dramatically influence the kinetics of water exchange on the complex. These results are in line with most of the general conclusions reported in literature concerning macrocyclic units attached to the well definite dendritic architecture with its higher degree of symmetry and rigidity than the hyperbranched and linear polymers macromolecular systems (7, 24, 29, 32).

This finding allows to predict water exchange rates for Gd(III) complexes attached to dendrons/dendrimers by determining this parameter for the monomeric chelate, before the tedious synthesis of whole molecule.

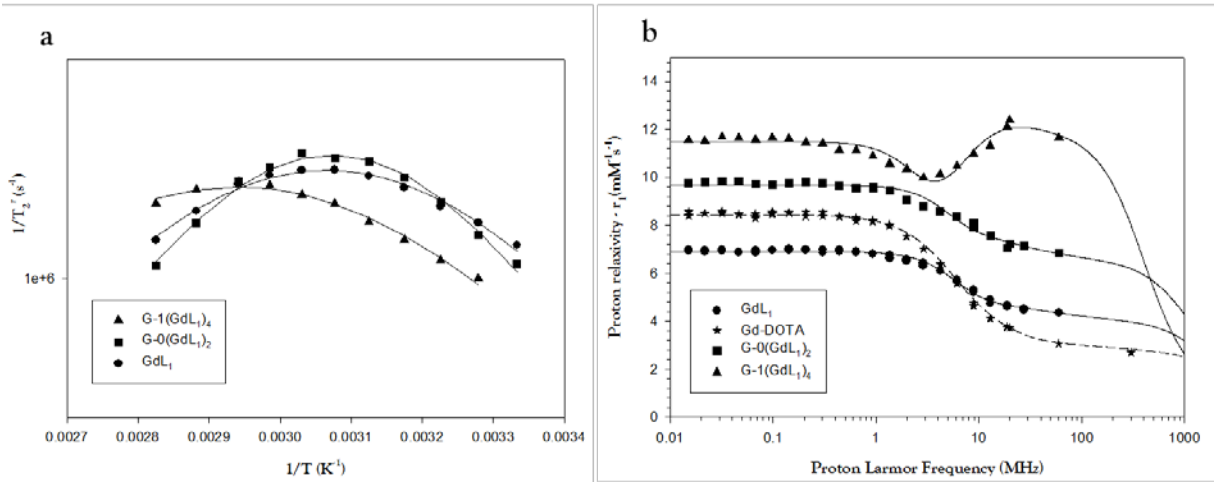

Figure 5 (a) Temperature dependence of the reduced ^{17}O transverse relaxation rate at 11.75 T; (b) comparison between ^{1}H NMRD profiles of **GdL_1** 1.78 mM (spheres), **G-0(GdL_1)$_2$** 1.59 mM (squares), **G-1(GdL_1)$_4$** 0.90 mM (triangles) and Gd-DOTA (stars). The lines represent simulation using the best-fit parameters (Table 1).

The most important expectation for the dendritic contrast agents was that the rotational correlation time, τ_R, which limits the proton relaxivity of current contrast agents at imaging fields, would be increased. The longer the rotational correlation time, the greater is the potential for a higher relaxivity of the agent. In our present study, we address the problem of the paramagnetic enhancement by increasing the molecular weight of the contrast agent. As expected for large molecules previously reported, and for these systems described in the present work, the values of the τ_R are higher than those found for monomeric Gd^{3+} complexes (Table 1), which results in an increase of the relaxivity mainly at high field where a hump can be observed on the NMRD profile of G-1(GdL_1)$_4$ (r_1 = 49.6 and 14.4 s^{-1} mM^{-1} for **G-1(GdL_1)$_4$** and **G-0(GdL_1)$_2$** respectively, at 20MHz (37 ° C)).

Table 1 Parameters of **GdL_1**, **G-0(GdL_1)$_2$** and **G-1(GdL_1)$_4$** obtained from the analysis of ^{17}O NMR and ^{1}H NMRD data compared with Gd-DOTA as a reference.

	Reference (35)	New Complexes		
Parameters	**Gd-DOTA**	**GdL_1**	**G-0(GdL_1)$_2$**	**G-1(GdL_1)$_4$**
r_1^b [mM^{-1} s^{-1}]	3.5	4.7	7.2	12.4

r_1^c [mM^{-1} s^{-1}]	3.5	4.7	14.4	49.6
τ_V^{310}(ps)	7 ± 1.0	19.2 ± 1.1 (23.8)[a]	22.6 ± 2.14 (22)[a]	47.1 ± 1.92 (6)[a]
τ_M^{310}(ns)	122 ± 10	331 ± 44	364 ± 22	541 ± 60
τ_R^{310}(ps)	53 ± 1.3	93.1 ± 2.2	152 ± 4.87	473 ± 10.9
τ_{S0}^{310}(ps)	404 ± 24	74.8 ± 1.2	72.0 ± 5.43	127 ± 1.63
q_{SS}			3.15 ± 0.108	-
τ_{SS}(ps)			18.3 ± 2.89	10.5 ± 49.8

(a) The first values were obtained from the fitting of the proton NMRD profile; the values in parentheses were obtained from the fitting of the ^{17}O NMRD data; (b) r_1 corresponds to the relaxivity per Gd-complex, (c) per molecule, both calculated at 20 MHz and 37 °C.

In vivo evaluation of biodistribution and contrast enhancing properties in tumour bearing mice

Biodistribution of the two investigated molecules was studied in healthy C57 mice at several time points following intravenous injection at doses of 0.05 mmol Gd/kg (Fig. 6, left). All the molecules were completely cleared from the vascular compartment 24h post their administration. A pronounced accumulation within the spleen was observed for all the two compounds, even the day after the administration, with similar contrast enhancements values 24h post injection, probably due to the large size of these compounds. A different distribution was observed within the liver, with higher contrast enhancement values for **G1(GdL$_1$)$_4$** in comparison to **G-0(GdL$_1$)$_2$**.

Fig. 6 (right) shows the dynamic signal intensity enhancements in the tumour regions of C57BL/6 mice transplanted subcutaneously with B16-F10 melanoma cells. Significant contrast enhancement was observed, already at 5 min post-injection, for **G-1(GdL$_1$)$_4$** and **G-0(GdL$_1$)$_2$**, of 42%, and 28%, respectively. The contrast enhancement slowly reduced thereafter for **G-1(GdL$_1$)$_4$**, while for **G-0(GdL$_1$)$_2$** remained quite constant along time. Measurements of relative area under the curve (AUC) clearly show a higher contrast enhancement inside the tumour region for **G-1(GdL$_1$)$_4$** that becomes more evident 30 min after the injection.

All the investigated CAs induced a good contrast enhancement in the tumour region, thanks to the enhanced permeability retention effect, at the investigated doses of 0.05 mmol Gd/kg (Fig. 7). **G-**

0(GdL$_1$)$_2$ showed the lower contrast enhancement and accumulation inside tumour region, despite almost no uptake in the liver. This can be explained by the small size of this system that results in faster wash-in and wash-out properties, combined with the lowest relaxivity efficiency. Conversely, **G-1(GdL$_1$)$_4$** showed a better contrast enhancement and accumulation within tumour.

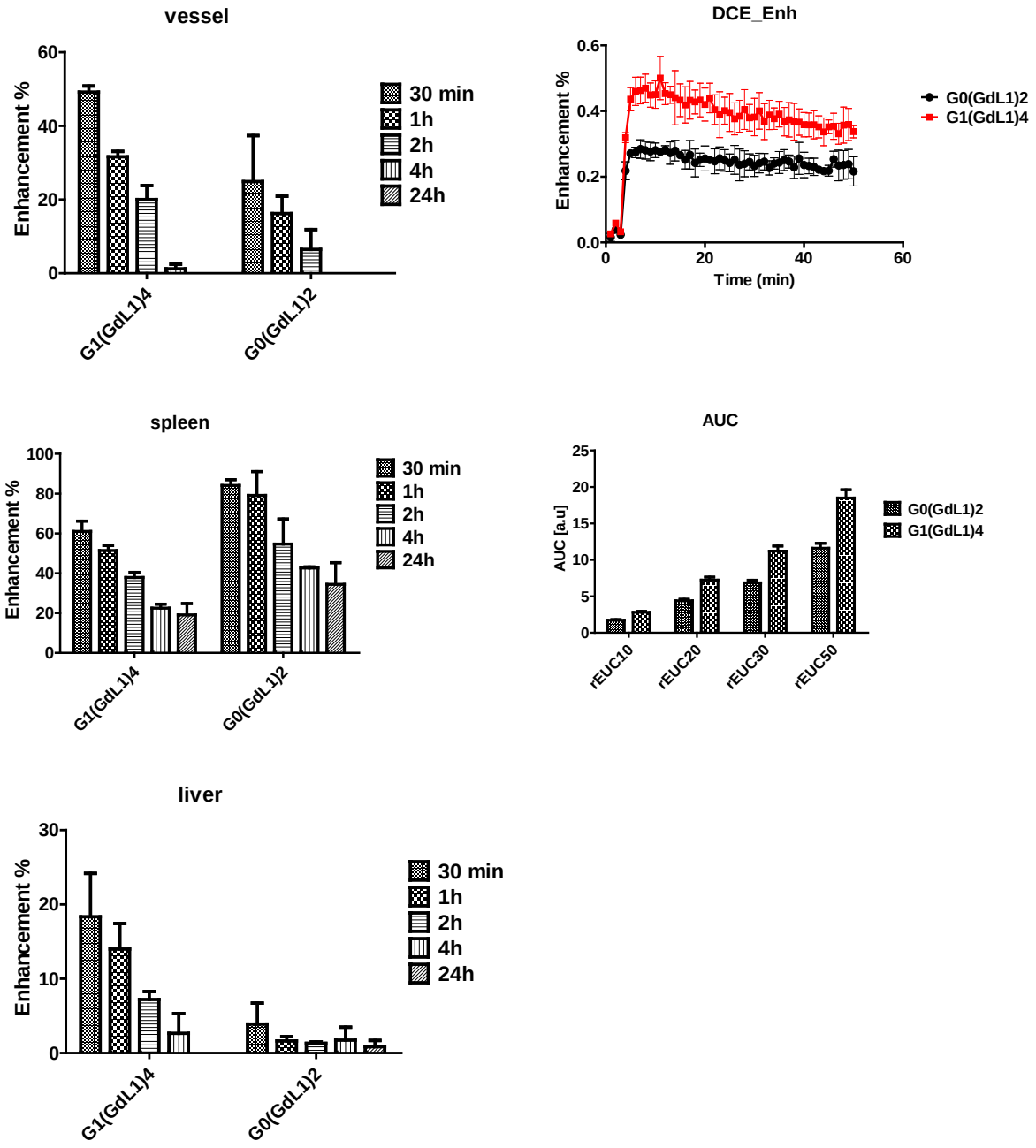

Figure 6: (Left): signal intensities contrast enhancements measured in the heart (top), spleen (middle) and liver (bottom) at various time points post-injection (30 min, 1h, 2h, 4h and 24h) of **G-1(GdL$_1$)$_4$** and **G-0(GdL$_1$)$_2$** at the same dose of 0.05 mmol Gd/kg. Values are shown as mean ±SD (n=2 mice) for each contrast agent; (Right): time course of MRI signal intensity

enhancement (top) and calculated area under the curve (AUC, bottom) in tumour bearing mice after intravenous injection of **G-0(GdL$_1$)$_2$** (black squares), and **G-1(GdL$_1$)$_4$** (red squares) at a dose of 0.05 mmol Gd/kg at several time points post injection 10, 20, 30 and 50 min. Values are shown as mean ±SD (n=3 mice) for each contrast agent.

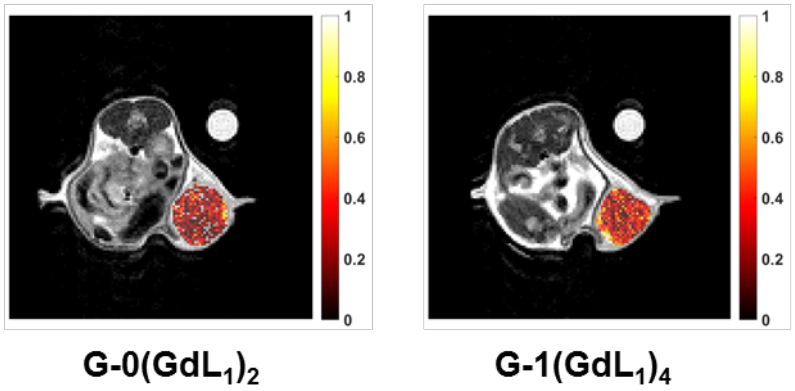

Figure 7: Representative tumour SI enhancement maps over imposed onto anatomical T_{2w} images upon injection of **G-0(GdL$_1$)$_2$**, and **G-1(GdL$_1$)$_4$** at a dose of 0.05 mmol Gd/kg.

Conclusions

A convenient methodology has been presented for the synthesis of poly[*N*,*N*-bis(3-aminopropyl)glycine] (PAPGly) dendrons Gd-based contrast agents for MR imaging. By orthogonal chemistries, a novel synthetic methodology has been developed to obtain two generations of PAPGly dendrons conjugated with a low molecular weight Gd-DO3A-based complex. The longitudinal (r_1) relaxivities of these MRI contrast agents increase along with their size, indicating a longer rotational correlation time for the high dendron generation. Consequently, very high relaxivities were observed (r_1 = 14.4 s^{-1} mM^{-1} and 49.6 s^{-1} mM^{-1} for the **G-0(GdL$_1$)$_2$** and **G-1(GdL$_1$)$_4$** per molecular complex, respectively). These values are significantly higher in comparison with parent monomeric **GdL$_1$** (r_1 = 4.7 s^{-1} mM^{-1}) complex and with the commercial one (Gd-DOTA, r_1 = 3.5 s^{-1} mM^{-1}). Our MRI results support the hypotheses that the Gd-based dendrons with high molecular weight, or macromolecular dendrimers Gd-complexes, can improve contrast enhancement as a result of its higher relaxivities comparing to the low molecular weight contrast agents. Furthermore, high structural and chemical homogeneity of the dendritic polymers can differ significantly from linear polymers in their properties. For example, biodistribution and pharmacokinetic properties can be tuned more easily by controlling dendrimer size and conformation.

Consequently, when those dendritic contrast agents are applied for DCE-MRI in mice they provide an opportunity to noninvasively extract important physiological and pathophysiological information.

Acknowledgements

This work was performed with the financial support of the FNRS, FEDER, the ARC, the Walloon Region (Gadolymph, Holocancer and Interreg projects), the Interuniversity Attraction Poles of the Belgian Federal Science Policy Office and the COST actions. Authors thank the Center for Microscopy and Molecular Imaging (CMMI, supported by European Regional Development Fund Wallonia).

Experimental Section

General methods and materials

All reagents and chemicals were obtained from commercial sources and used without further purification. Solvents were distilled and/or dried prior to use by standard methodology except for those, which were reagent grades. Water was demineralized prior to use. Unless stated otherwise, all the reactions were carried out under a nitrogen atmosphere and the reaction flasks were pre-dried by heat gun under vacuum. The pH values of the samples were measured at ambient temperature using a Corning 125 pH meter with a calibrated micro-combination electrode purchased from Aldrich. The pH values of the solution were adjusted using aqueous solution 1M NaOH, 1N pyridine or 1N HCl. Most of the reactions were monitored by TLC on silica plates detecting the components by UV light or by applying the Dragendorff reagent, while other product formations were monitored via analytical HPLC (Waters W600, with a quaternary pump gradient module) with an UV detector coupled with a Waters Micromass ZQ system (Waters, Belgium). For low molecular weight characterization, ESI-QTOF-MS were obtained on a Q-TOF Ultima GLOBAL mass spectrometer (Waters-Micromass, Manchester, UK), whereas for high molecular weight products, MALDI spectra were obtained on MALDI-TOF spectrometer (Waters-Micromass, Manchester, UK).

The purification of the compounds was performed on KP-silica and KP-C18 Biotage cartridges over a Biotage flash chromatography instrument, Uppsala, Sweden. ^{1}H-NMR, ^{13}C-NMR spectra were recorded on either a Bruker Avance-300 MHz or a Bruker Avance II-500 MHz spectrometer, at 25°C. Chemical shifts are given in ppm (δ) values. Data are reported as follows: chemical shift (multiplicity: s = singlet, d = doublet, t = triplet, q = quadruplet, m = multiplet, br = broad resonance) J = coupling constant (Hz), integration, peak assignment in italic form.

Signal Intensity Enhancements in different organs were calculated by using ImageJ and drawing ROIs encompassing the whole organs. All the DCE-MRI images were analysed using in-house developed software in MatLab (MathWorks, Natick, MA). Relative Area Under the Curve (AUC) were calculated

by integrating the signal intensity enhancements along the time curve at different time points post Gd-compounds injections.

Synthesis of bis-(3-tert-butoxycarbonyl-aminopropyl) amine (2)

To a solution of the bis-(3-aminopropyl) amine **1** (10 g, 0.0762 moli) in DMF (75 ml) was added tert-butyl phenyl carbonate (32.63 g, 0.168 moli) (75). The reaction mixture was stirred for 40h at rt. and poured into a phosphate buffer (1L; 0.025 M K_2HPO_4 and 0.025 M NaH_2PO4). The pH was adjusted to 3 with aq. H_2SO_4 (2M) and mixture was extracted with CH_2Cl_2 (2x250 ml). The aq. phase was made strongly alkaline with aq. NaOH (9M) and extracted with CH_2Cl_2 (3x250 ml). The organic phase was dried (Na_2SO_4), filtered and concentrated in vacuo. The residual solvents (DMF and H_2O) were removed by drying the protected amine at less than 0.1 mmHg at 40 °C, to obtain a white solid compound **2** (18.9 g, 75% of yield). ESI MS: *m/z* 332 $[M + H]^+$; ^{1}H NMR (300 MHz, $CDCl_3$, 25 °C): δ 1.35 (s, 18 H), 1.58 (4H, q, 2x$CH_2CH_2CH_2$), 2.06 (2H, br s, 2xCONH), 2.57 (4H, t, 2x$NHCH_2CH_2$), 3.11 (4H, br t, 2x$CONHCH_2$), 5.32 (1H, br s, $NHCH_2$). ^{13}C NMR (300 MHz, $CDCl_3$, 25 °C): δ 28.35, 29.60, 38.68, 47.16, 77.88, 156.16.

Synthesis of benzyl N,N-bis {3-[(tert-butoxycarbonyl) amino] propyl} glycinate (3)

Compound **2** (6.78 g, 0.02 mol) and 10 ml DMF were dissolved in a three-necked flask under stirring. The mixture was cooled by using an ice bath followed by addition of benzyl bromo-acetate (4 ml, 0.025 mol) and DIPEA (3.5 ml, 0.02 mol) over a time period of 30 min. The resulting reaction mixture was stirred at 0 °C for additional 30 min, whereupon it was allowed to reach rt. The reaction mixture was reacted for additional 4h at rt. Ether (70 ml) was added and the formed white precipitate was collected by filtration, while the mother liquid was evaporated to dryness. The produced oil was dissolved in 70 ml DCM and carefully washed sequentially with 3 x 50 ml water, 2 x 50 ml 1M HCl, and 3 x 50 ml water. The organic phase was dried over Na_2SO_4 followed by evaporation to dryness. The crude product was purified by silica gel column chromatography using EtOAc/Heptane (70:30) as eluent, and the pure product **3** was obtained in a yield of 90%, 8.63 g. ESI MS: *m/z* 480 $[M + H]^+$; ^{1}H NMR (300 MHz, $CDCl_3$, 25 °C): δ 1.45 [18H, s, 2x$C(CH_3)_3$], 1.65 (4H, br s, 2x$CH_2CH_2CH_2$), 2.62 (4H, br s, 2xNCH_2CH_2), 3.18 (4H, br t, 2xCH_2CH_2NH), 3.37 (2H, br s, $COCH_2N$), 5.17 (2H, s, $COCH_2Ar$), 5.24 (2H, br s, 2xCONH), 7.37 (5H, br s, ArH_5). ^{13}C NMR (300 MHz, $CDCl_3$, 25 °C): δ 27.32, 28.45, 38.79, 52.11, 55.03, 66.30, 78.82, 128.37, 128.39, 128.59, 135.67, 156.10, 171.33.

Synthesis of N,N-bis{3-[(tert-butoxycarbonyl) amino] propyl} glycine (4)

Compound **3** (2.1 g, 4.37 mmol), Pd/C 10% (324 mg) and 100 ml MeOH were mixed in a sealed tube, whereupon hydrogen pressure of 60 psi was applied. The mixture was reacted 22h at rt. The resulting reaction mixture was filtered through a Celite pad and carefully washed with 150 ml MeOH. The mother liquid was evaporated to dryness, and white product **4** was obtained in a yield of 1.6 g. ESI MS: *m/z* 390 $[M + H]^+$; ^{1}H NMR (300 MHz, CD_3OD, 25 °C): δ 1.45 [18H, s, 2xC(CH_3)$_3$], 1.91 (4H, br s, 2x$CH_2CH_2CH_2$), 3.17 (4H, br s, 2xNCH_2CH_2), 3.36 (4H, br t, 2xCH_2CH_2NH), 3.69 (2H, br s, $COCH_2N$). ^{13}C NMR (300 MHz, CD_3OD, 25 °C): δ 26.04, 28.84, 38.23, 54.54, 56.78, 80.33, 158.74, 170.07.

Synthesis of N,N-bis(3-aminopropyl) glycine (G-0)

In a round bottom flask, compound **4** (1.0 g, 2.1 mmol) was dissolved in 20 ml of 50% solution of TFA in dry DCM, whereupon the mixture was stirred for 24h at rt. The reaction mixture was evaporated to dryness under reduced pressure, and the crude product was washed 2 times with ethyl ether (in a sonic bath) in order to remove further impurities, to give the compound **G-0** (1.358 g, pale-white colour, TFA-salt). ESI MS: *m/z* 280 $[M + H]^+$; ^{1}H NMR (300 MHz, $CDCl_3$, 25 °C): δ 1.69 (4H, q, 2x$CH_2CH_2CH_2$), 2.56 (4H, t, 2xNCH_2CH_2), 2.71 (4H, t, 2x$CH_2CH_2NH_2$), 3.86 (2H, s, $COCH_2N$). ^{13}C NMR (300 MHz, $CDCl_3$, 25 °C): δ 23.94, 38.40, 53.15, 55.02, 69.02, 129.69, 129.71, 129.75, 136.43, 169.38.

Synthesis of G-0(L_1)$_2$

Compound **G-0** (190 mg, 0.456 mmol) was dissolved in water (25 ml), and the pH was adjusted to 9-10 with diluted NaOH aqueous solution. **DO3A-NCSPP** (771 mg, 1.44 mmol) freshly prepared as previously reported in chapter 3, was added, and the reaction mixture was stirred at room temperature for 48 h. The solution was freeze-dried to get a yellow powder (832 mg). A portion of crude compound (100 mg) was purified by using a semi-preparative HPLC condition: RP-C18 column; CH_3CN/H_2O (buffer NH_4HCO_3, pH=7.5) as mobile phase; gradient 5-30% CH_3CN in 30 min with a flow rate 1 ml/min; to obtain 70 mg of pure pale-yellow compound **G-0(L_1)$_2$**. ESI MS: *m/z* 1261 $[M + H]^+$; ^{1}H NMR (500 MHz, D_2O, 25 °C): δ 1.22 (6H, br s, 2xCH_3CHCO), 1.97 (4H, br s, $CH_2CH_2CH_2$), 2.82-3.91 (54H, 2 br m), 4.81 (2H, br s, 2xCH_3CHCO), 7.31 and 7.70 (8H, 2 br d, Ar*H*). ^{13}C NMR (500 MHz, D_2O, 25 °C): δ 13.10, 23.67, 41.09, 44.07, 45.24, 48.88, 50.89, 51.50, 52.71, 54.87, 55.68, 56.57, 56.93, 100.00, 123.37, 129.80, 132.21, 142.48, 169.56, 170.35, 170.54, 177.07, 179.97, 203.07.

Synthesis of benzyl N,N-bis(3-aminopropyl) glycinate (5)

In a round bottom flask, compound **3** (1.1 g, 2.3 mmol) was dissolved in 20 ml of 50% solution of TFA in dry DCM, whereupon the mixture was stirred for 24h at rt. The reaction mixture was evaporated to dryness under reduced pressure, and the crude product was washed 2 times with ethyl ether (in a sonic bath) in order to remove further impurities, to give the compound **5** (1.58 g, pale-white colour, TFA-salt). ESI MS: *m/z* 280 $[M + H]^+$; ^{1}H NMR (300 MHz, $CDCl_3$, 25 °C): δ 2.09 (4H, q, 2x$CH_2CH_2CH_2$), 3.06 (4H, t, 2xNCH_2CH_2), 3.21 (4H, t, 2x$CH_2CH_2NH_2$), 4.06 (2H, s, $COCH_2N$), 5.27 (2H, s, $COCH_2Ar$), 7.37 (5H, m, ArH_5). ^{13}C NMR (300 MHz, $CDCl_3$, 25 °C): δ 23.94, 38.40, 53.15, 55.02, 69.02, 129.69, 129.71, 129.75, 136.43, 169.38.

Synthesis of benzyl N,N-bis{3-[(N,N-bis{3-[(tert-butoxycarbonyl) amino] propyl} glycyl) amino] propyl} glycinate (6)

Into a two-necked round bottom flask, under dry condition (N_2), a suspension of compound **4** (1.1 g, 2.82 mmol), 3 eq. of 1-[Bis(dimethylamino)methylene]-1*H*-1,2,3-triazolo[4,5-*b*]pyridinium 3-oxid hexafluorophosphate (HATU) (1.289 g, 3.39 mmol), and 2.5 eq. of DIPEA (0.365 g, 2.83 mmol) in CH_3CN HPLC-grade (70 ml) was stirred for 30 min at RT. Benzyl *N,N*-bis(3-aminopropyl) glycinate (TFA-salt) (**5**) (0.7 g, 1.13 mmol) was first dissolved in 20 ml of CH_3CN with 4 eq. of DIPEA, and added dropwise to the reaction mixture over 30 min, [reaction monitored by TLC: CH_2Cl_2/CH_3OH, 9:1, with a ninhydrin test]. After 5 h, the reaction was stopped and poured into ethyl acetate (150 ml). The organic layer was first washed three times with saturate $NaHCO_3$ solution, and then three times with H_2O, dried over Na_2SO_4, and evaporated to dryness to give a pale-white oil compound (1.342 g). A 1.2 g aliquot of residue product was purified by flash chromatography on silica gel using CH_2Cl_2/CH_3OH (9.5:0.5) as mobile phase. After evaporation of the solvent, 812 mg (0.77 mmol, with 75.4 % of total yield) of **6** was obtained as a white crystal compound. ESI MS: *m/z* 1055 $[M + H]^+$; ^{1}H NMR (300 MHz, $CDCl_3$, 25 °C): δ 1.42 [36H, s, 4x$C(CH_3)_3$], 1.62 (12H, br m, 6x$CH_2CH_2CH_2$), 2.48 (8H, t, 4xNCH_2CH_2), 2.61 (4H, t, 2xNCH_2CH_2), 3.00 (4H, s, 2xNCH_2COONH), 3.13 (8H, q, 4xCH_2CH_2NHCOOtert-But), 3.31 (4H, q, 2xCH_2CH_2NHCO), 3.37 (2H, s, NCH_2COOCH_2), 5.12 (2H, s, $COCH_2Ar$), 7.32 (5H, br m, ArH_5). ^{13}C NMR (300 MHz, $CDCl_3$, 25 °C): δ 27.63, 27.68, 28.43, 37.14, 38.53, 51.85, 52.66, 54.91, 58.52, 66.16, 79.03, 100.00, 128.19, 128.27, 128.55, 135.75, 156.06, 171.31, 171.38.

Synthesis of N,N-bis(3-{[N,N-bis(3-aminopropyl)glycyl]amino}propyl)glycine (G-1)

The dendron **G-1** (156 mg, 0.29 mmol) was obtained after a completely deprotection of compound **6** (325 mg, 0.31 mmol) by using the same reaction conditions as described for the synthesis of dendron **G-0**. ESI MS: *m/z* 532 $[M + H]^+$; ^1H NMR (300 MHz, $CDCl_3$, 25 °C): δ 1.72 (12H, br m, 6x$CH_2CH_2CH_2$), 2.45 (8H, t, 4xNCH_2CH_2), 2.61 (4H, t, 2xNCH_2CH_2), 2.83 (8H, q, 4x$CH_2CH_2NH_2$), 3.10 (4H, s, 2xNCH_2CONH), 3.31 (4H, q, 2xCH_2CH_2NHCO), 3.73 (2H, s, NCH_2COOH). ^{13}C NMR (300 MHz, $CDCl_3$, 25 °C): δ 27.08, 30.43, 37.14, 38.53, 51.85, 52.66, 54.91, 58.52, 170.31, 173.38.

Synthesis of G-1(L$_1$)$_4$

Compound **G-1** (156 mg, 0.29 mmol) was dissolved in water (20 ml), and the pH was adjusted to 9-10 with diluted NaOH aqueous solution. **DO3A-NCSPP** (770 mg, 1.43 mmol) freshly prepared as previously reported in chapter 3, was added, and the reaction mixture was stirred at room temperature for 48 h. The crude product was purified at pH = 7, by ultrafiltration using a membrane with a molecular weight cut-off of 1 kDa, to get a pale yellow solid of 0.2 g. MALDI Q-TOF: *m/z* 2673 $[M + H]^+$; ^1H NMR (500 MHz, D_2O, 25 °C): δ 1.31 (12H, br s, 4xCH_3CHN), 1.78-1.95 (12H, br d, 6x$CH_2CH_2CH_2$), 2.91-4.00 (122H, br m), 7.42-7.91 (16H, 2br m, 4xArH_4). ^{13}C NMR (500 MHz, D_2O, 25 °C): δ 12.95, 13.30, 23.73, 24.05, 36.39, 41.50, 44.12, 45.28, 48.25, 50.91, 51.54, 52.45, 52.86, 55.45, 56.64, 56.96, 62.50, 72.06, 122.74, 129.74, 131.77, 142.84, 142.97, 169.53, 170.10, 170.50, 177.78, 179.71, 202.78.

Preparation of G-0(GdL$_1$)$_2$ and G-1(GdL$_1$)$_4$ dendrons complexes

The dendrons **G-0(GdL$_1$)$_2$** and **G-1(GdL$_1$)$_4$** complexes were prepared by a stepwise addition of $GdCl_3 \cdot 6H_2O$ to a solution of 83 mg (0.066 mmol) and 71 mg (0.026 mmol) of **G-0(L$_1$)$_2$** and **G-1(L$_1$)$_4$** respectively, in 5 ml of H_2O, maintaining the pH between 6.5 and 7.0 by addition of 1 M NaOH aqueous solution. After 4 days the reaction mixture was stopped, and the excess of free lanthanide for the **G-0(GdL$_1$)$_2$** complex was removed by centrifugation as $Gd(OH)_3$ precipitate, which appeared at pH 10 after addition of 1 M NaOH, whereas for **G-1(GdL$_1$)$_4$** complex the excess of free gadolinium was removed by ultra-filtration using a membrane with a cut-off of 3 kDa. The absence of free Gd^{3+} ions was confirmed by a xylenol orange test, with a final pH of both solutions around 6.5-7.00. The solutions were freeze-dried to give a pale-yellow solid for both final complexes: **G-0(GdL$_1$)$_2$** 95 mg, ESI MS: *m/z* 1569 $[M + H]^+$; and 75 mg **G-1(GdL$_1$)$_4$**, MALDI Q-TOF: *m/z* 3290 $[M + H]^+$.

NMRD profiles

$1/T_1$ ^{1}H NMRD profiles were measured on a Stelar Spinmaster FFC fast field cycling NMR relaxometer (Stelar, Mede, Pavia, Italy) over a range of magnetic fields extending from 0.24 mT to 0.7 T and corresponding to ^{1}H Larmor frequencies from 0.01 to 30 MHz using 0.6 ml samples in 10 mm o.d. tubes. The samples were prepared by dissolution of appropriate amounts of freeze-dried complexes of **GdL$_1$**, **G-0(GdL$_1$)$_2$**, and **G-1(GdL$_1$)$_4$** in Milli-Q water with the pH in the range 6.5-7.0. The exact Gd^{3+} concentration was determined by proton relaxivity measurements at 20 MHz and 37 °C after complete hydrolysis in concentrated HNO_3. Additional relaxation rates at 20 and 60 MHz were obtained with Bruker Minispec mq-20 and mq-60 spectrometers (Bruker, Karlsruhe, Germany), respectively. The 300 MHz data were obtained on a Bruker Avance-300 high resolution spectrometer.

Fitting of the ^{1}H NMRD was performed with data processing software that uses different theoretical models describing observed nuclear relaxation phenomena (Minuit, CERN Library) (36, 37). The theoretical model takes into account the inner-sphere interaction, the outer-sphere interaction and when necessary the second sphere contribution (7).

^{17}O NMR studies

^{17}O NMR relaxation rate measurements were performed on a Bruker Avance II-500 spectrometer using 5 mm diameter sample tubes containing 325 µl (pH 6.5-7.00) of **G-0(GdL$_1$)$_2$** (25.5 mM) and **G-1(GdL$_1$)$_4$** (15.9 mM) solutions. The temperature was regulated by air or N_2 flow controlled by a BVT-3200 unit. ^{17}O transverse relaxation times of pure water (diamagnetic contribution) were measured using a CPMG sequence and a subsequent two-parameter fit of the data points. The 90 and 180° pulse lengths were 27.5 and 55 µs, respectively. Broadband proton decoupling was applied during the acquisition of all ^{17}O NMR spectra. ^{17}O T_2 of water in complex solution was obtained from line width measurement. The data are presented as the reduced transverse relaxation rate $1/T_2^R = 55{:}55/([\text{Gd complex}]\cdot q \cdot T_2^P)$, where [Gd complex] is the molar concentration of the complex, q is the number of coordinated water molecules and T_2^P is the paramagnetic transverse relaxation rate obtained after subtraction of the diamagnetic contribution from the observed relaxation rate. The number of water molecules in the first coordination sphere (q) of the Gd^{3+} complex **G-0(GdL$_1$)$_2$** and **G-1(GdL$_1$)$_4$** was determined at 60 °C using a Bruker Avance II-500 spectrometer. The tubes with 5 mm external diameter containing 300 µl of the sample with 50 µl of D_2O for the lock were used for the measurements. The hydration number q was obtained by comparing the ^{17}O NMR chemical shifts of **G-0(GdL$_1$)$_2$** and **G-1(GdL$_1$)$_4$** with those of Gd-DOTA and Gd-DTPA (q=1) (7, 38).

In vivo studies

Mice

6-old-week male C57BL/6 mice (n=3 for each molecule) were inoculated subcutaneously with 3×10^5 B16-F10 cell in 100 µL of PBS on both flanks. C57BL/6 mice (Charles River Laboratories Italia S.r.l., Calco Italia) were maintained under specific pathogen free conditions in the animal facility of the Molecular Biotechnology Center, University of Torino, and treated in accordance with the EU guidelines (EU2010/63). All in vivo studies were conducted according to approved procedures of the Institutional Animal Care and Use Committee of the University of Torino. Before imaging, mice were anaesthetized with a mixture of tiletamine/zolazepam (Zoletil 100; Vibac, Milan, Italy) 20mg/kg and xylazine (Rompun; Bayer, Milan, Italy) 5mg/kg and during the acquisition their breath rate was monitored throughout in vivo MRI experiments using a respiratory probe. Cannulation of the lateral tail vein with a catheter was exploited for intravenous injection of the investigated molecules.

DCE-MRI experiments

Mice were placed supine in a solenoid Tx/Rx coil with an inner diameter of 3.5 cm. The breath rate was monitored throughout in vivo MRI experiments using a respiratory probe (SAII Instruments, Stony Brook, NY - USA). MR images were acquired with a 1 Tesla Aspect M2 MRI scanner (Aspect Magnet Technologies Ltd., Israel). After the scout image acquisition, a T_2-weighted (T2w) anatomical image was acquired with a Fast Spin Echo sequence (TR 2500 ms; TE 44ms; number of slices 10; slice thickness 1.5 mm; FOV 40 mm; matrix 152 × 160; four averages; acquisition time 3 m 20 s). The DCE-MRI dynamic protocol consisted of the application of an axial T_1-weighted (T_1w) 3D spoiled Gradient Echo sequence with 3 initial pre-contrast images acquisition that were followed by the injection through the catheter of one of the two investigated compounds at the same dose of 0.05 mmolGd/kg. After injection, 47 dynamic post-contrast images were acquired with the following parameters: TR = 40 ms; TE = 2.1 ms, flip angle = 60°, number of slices = 10, slice thickness = 1.5 mm, FOV = 40 mm, matrix = 128 × 128, acquisition time 58 s.

All the DCE-MRI images were analysed using in-house developed software in MatLab (MathWorks, Natick, MA) .

Biodistribution

6-old-week male C57BL/6 mice (n=2 for each molecule) were administered with the two dendrons Gd-based contrast agents at a dose of 0.05 mmol Gd/kg. T1w images were acquired before and after i.v. injection at several time points: 30 min, 1h, 2h, 4h and 24h. Region of interests (ROIs) were manually

placed in several organs (liver, spleen, major vessel) and signal intensity (SI) values were measured and contrast enhancement calculated as (SIpost-SIpre)/SIpre.

References

1. S. Kunjachan, J. Ehling, G. Storm, 1. Kiessling, T. Lammers, 'Noninvasive Imaging of Nanomedicines and Nanotheranostics: Principles, Progress, and Prospects', *Chem Rev* **2015**, *115(19)*, 10907-10937.
2. N. K. Logothetis, 'What we can do and what we cannot do with fMRI', *Nature* **2008**, *453(7197)*, 869-878.
3. H. Kobayashi, et al. 'Rapid accumulation and internalization of radiolabeled herceptin in an inflammatory breast cancer xenograft with vasculogenic mimicry predicted by the contrast-enhanced dynamic MRI with the macromolecular contrast agent G6-(1B4M-Gd)(256)', *Cancer Res* **2002**, *62(3)*, 860-866.
4. L. J. De Cocker, A. Lindenholz, J. J. Zwanenburg, A. G. Van der Kolk, M. Zwartbol, P. R. Luijten, ' Clinical vascular imaging in the brain at 7T', *Neuroimage* **2016**, In press.
5. P. Caravan, C. T. Farrar, L. Frullano, R. Uppal, 'Influence of molecular parameters and increasing magnetic field strength on relaxivity of gadolinium- and manganese-based T1 contrast agents', *Contrast Media Mol Imaging* **2009**, *4*, 89-100.
6. S. Laurent, D. Forge, M. Port, A. Roch, C. Robic, L. Vander Elst, R. N. Muller, 'Magnetic Iron Oxide Nanoparticles: Synthesis, Stabilization, Vectorization, Physicochemical Characterizations, and Biological Applications', *Chem Rev* **2008**, *108*, 2064-2110.
7. A. S. Merbach, L. Helm, E. Tóth, 'The Chemistry of Contrast Agents in Medical Magnetic Resonance Imaging, Second Edition', *John Wiley & Sons* **2013**.
8. H. Daldrup, D. M. Shames, M. Wendland, Y. Okuhata, T. M. Link, W. Rosenau, Y. Lu, R. C. Brasch, 'Correlation of Dynamic Contrast-enhanced MR Imaging with Histologic Tumor Grade: Comparison of Macromolecular and Small-molecular Contrast Media', *Am J Roentgenol* **1998**, *171*, 941-949
9. P. Caravan, 'Strategies for increasing the sensitivity of gadolinium based MRI contrast agents', *Chem Soc Rev*, **2006**, *35*, 512-523.
10. L. Granato, S. Laurent, L. Vander Elst, K. Djanashvili, J. A. Peters, R. N. Muller, 'The Gd^{3+} complex of 1,4,7,10-tetraazacyclododecane-1,4,7,10-tetraacetic acid mono(p-isothiocyanatoanilide) conjugated to inulin: a potential stable macromolecular contrast agent for MRI', *Contrast Media Mol Imaging*, **2011**, *6*, 482-491.
11. T. H. Helbich, A. Gossman, P. A. Mareski, B. Radüchel, T. P. Roberts, D. M. Shames, M. Mühler, K. Turetschek, R. C. Brasch, 'A new polysaccharide macromolecular contrast agent for MR imaging: biodistribution and imaging characteristics', *J Magn Reson Imaging*, **2000**, *11(6)*, 694-701.
12. P. Loubeyre et al. 'Carboxymethyl-Dextran-Gadolinium-Dtpa as a Blood-Pool Contrast Agent for Magnetic Resonance Angiography Experimental Study in Rabbits', *Invest Radiol*, **1996**, *31 (5)*, 288-293.
13. G. Schuhmann-Giampieri, H. Schmitt-Willich, T. Frenzel, W.-R. Press, H.-J. Weinmann, 'In Vivo and In Vitro Evaluation of Gd-DTPA-Polylysine as a Macromolecular Contrast Agent for Magnetic Resonance Imaging', *Invest Radiol*, **1991**, *26(11)*, 969-974.

14. M. Ogawa, C.A. Regino, B. Marcelino, M. Williams, N. Kosaka, L. H. Bryant, P. L. Choyke, H. Kobayashi, 'New nanosized biocompatible MR contrast agents based on lysine-dendri-graft macromolecules', *Bioconjug Chem*, **2010**, *21*, 955-960.
15. L. H. Jr. Bryant, M. W. Brechbiel, C. Wu, J. W. Bulte, V. Herynek, J. A. Frank, 'Synthesis and relaxometry of highgeneration (G=5, 7, 9, and 10) PAMAM dendrimer-DOTA-gadolinium chelates', *J Magn Reson Imaging*, **1999**, *9*, 348-352.
16. H. Kobayashi, and al. '3D-micro-MR angiography of mice using macromolecular MR contrast agents with polyamidoamine dendrimer core with reference to their pharmacokinetic properties', *Magn Reson Med*, **2001**, *45*, 454-460.
17. H. Kobayashi, et al. 'Micro-MR angiography of normal and intratumoral vessels in mice using dedicated intravascular MR contrast agents with high generation of polyamidoamine dendrimer core: reference to pharmacokinetic properties of dendrimer-based-MR contrast agents', *J Magn Reson Imaging,* **2001**, *14*, 705-713.
18. B. Klajnert, L. Peng, V. Cena, 'Dendrimers in Biomedical Applications', *Royal Society of Chemistry*, **2013**.
19. R. B. Lauffer, 'Paramagnetic Metal Complexes as Water Proton Relaxation Agents for NMR Imaging: Theory and Design', *Chem Rev*, **1987**, *87*, 901-927.
20. S. Aime, S. Geninatti Crich, E. Gianolio, G. B. Giovenzana, L. Tei, E. Terreno, 'High sensitivity lanthanide(III) based probes for MR-medical imaging', *Coord Chem Rev*, **2006**, *250*, 1562-1579.
21. P. Caravan, 'Protein-targeted gadolinium-based magnetic resonance imaging (MRI) contrast agents: design and mechanism of action', *Acc Chem Res*, **2009,** *42(7)*, 851-862.
22. G. Adam, J. Neuerburg, E. Spuntrup, A. Muhler, K. Scherer, R. W. Gunther, 'Gd-DTPA-cascade-polymer-potential blood-pool contrast agent for MR-imaging', *J Magn Reson Imaging*, **1994**, *4*, 462-466.
23. E. C. Wiener, M. W. Brechbiel, H. Brothers, R. L. Magin, O. A. Gansow, D. A. Tomalia, P.C. Lauterbur, 'Dendrimer-based metal chelates: A new class of magnetic resonance imaging contrast agents', *Magn Reson Med*, **1994**, *31(1)*, 1-8.
24. V. J. Venditto, C. A. Regino, M. W. Brechbiel, 'PAMAM dendrimer based macromolecules as improved contrast agents', *Mol Pharm*, **2005**, *2(4)*, 302-311.
25. S. Langereis, Q. G. De Lussanet, M. H. P. Van Genderen, W. H. Backes, E. W. Meijer, 'Multivalent contrast agents based on gadolinium− diethylenetriaminepentaacetic acid-terminated poly (propylene imine) dendrimers for magnetic resonance imaging', *Macromolecules,* **2004**, *37(9)*, 3084-3091.
26. S. Langereis, et al. 'Evaluation of Gd(III)DTPA-terminated poly(propylene imine) dendrimers as contrast agents for MR imaging', *NMR Biomed*, **2006**, *19*, 133-141.
27. K. Luo, G. Liu, W. She, Q. Wang, G. Wang, B. He, H. Ai, Q. Gong, B. Song, Z. Gu, 'Gadolinium-labeled peptide dendrimers with controlled structures as potential magnetic resonance imaging contrast agents', *Biomaterials*, **2011**, *32(31)*, 7951-7960.
28 E. Toth, D. Pubanz, S. Vauthey, L. Helm, A. E. Merbach, 'High-pressure NMR kinetics. 72. The role of water exchange in attaining maximum relaxivities for dendrimeric MRI contrast agents', *Chem Eur J,* **1996**, *2*, 1607-1615.
29. J. Rudovsky, P. Hermann, M. Botta, S. Aime, I. Lukes, 'Dendrimeric Gd(III) complex of a monophosphinated DOTA analogue: optimizing relaxivity by reducing internal motion', *Chem Commun*, **2005**, *18*, 2390-2392.
30. A. J. L. Villaraza, A. Bumb, M. W. Brechbiel, 'Macromolecules, dendrimers, and nanomaterials in magnetic resonance imaging: the interplay between size, function, and pharmacokinetics', *Chem Rev*, **2010**, *110*, 2921-2959

31. H. Kobayashi, M. W. Brechbiel, 'Nano-sized MRI contrast agents with dendrimer cores', *Adv Drug Deliv Rev*, **2005**, *57*, 2271-2286.
32. H. Kobayashi, M. W. Brechbiel, 'Dendrimer-based macromolecular MRI contrast agents: characteristics and application', *Mol Imaging,* **2003**, *2*, 1- 10.
33. L. Granato, L. Vander Elst, C. Henoumont, R. N. Muller, S. Laurent, 'Optimizing Water Exchange Rates and Rotational Mobility for High-Relaxivity of a Novel Gd-DO3A Derivative Complex Conjugated to Inulin as Macromolecular Contrast Agents for MRI', *Chemistry and Biodiversity*, **2018**, *15(2)* e1700487 .
34. P. Herman, J. Kotek, V. Kubíček, I. Lukeš, 'Gadolinium(III) complexes as MRI contrast agents: ligand design and properties of the complexes', *Dalton Trans*, **2008**, 3027-3047.
35. S. Laurent, L. Vander Elst, R. N. Muller, 'Comparative study of the physicochemical properties of six clinical low molecular weight gadolinium contrast agents', *Contrast Med. Mol. Imaging*, **2006**, *1(3)*, 128-137.
36. R. N. Muller, D. Declercq, P. Vallet, F. Giberto, B. Daminet, H. W. Fisher, F. Maton, Y. Van Haverbeke, 'Proceedings of ESMRMB', *7th Annual Congress*, **1990**, *394*.
37. P. Vallet, 'Relaxivity of nitroxide stable free radicals. Evaluation by field cycling method and optimisation' *PhD Thesis, University of Mons*, **1992**.
38. C. M. Alpoim, A. M. Urbano, C. F. G. C. Geraldes, J. A. Peters, 'Determination of the number of inner-sphere water molecules in lanthanide (III) Polyaminocarboxylate complexes', *J Chem Soc Dalton Trans,* **1992**, 463-467.

.